ADVANCED ENERGY & SUSTAINABILITY RESEARCH
Open Access
www.advenergysustres.com

Effects of the Operating Point of Photovoltaic Strings on Sizing of DC- and AC-Connected Energy Storage Systems for Power Smoothing

Kari Lappalainen

Photovoltaic (PV) power generators are constantly exposed to operating condition variations. While the electrical characteristic of a PV generator has exactly one maximum power point (MPP) during homogeneous operating conditions, several MPPs may exist during nonuniform operating conditions. Since highly varying global MPP voltage causes large fluctuations in the inverter reference voltage, it would be beneficial to keep the operating point of the inverter all the time close to the nominal MPP voltage to secure more predictable and straightforward operation of the PV system. This article presents a study of the effects of the operating point on the operation of PV strings equipped with energy storage systems (ESS). A scenario in which the MPP closest to the nominal MPP voltage is used as the operating point is compared to operation in the global MPP. The effects of inverter sizing on the selection of the operating point are also studied. Moreover, DC and AC connections of the ESSs are compared. The study is based on measured current–voltage curves of a 23 module PV string. The results show that, in practice, there are no major differences in sizing of DC-connected ESSs between the two MPPs.

1. Introduction

Photovoltaic (PV) systems face continual variation in their operating conditions. Especially, variations in irradiance can be very strong and steep.[1] Under homogeneous operating conditions, the current–voltage (I–U) curve of a PV generator has exactly one maximum power point (MPP). However, if a PV generator is operating under nonuniform operating conditions, for example, due to partial shading, the PV cells and modules of the generator have divergent electrical characteristics, and as a result, there may be several MPPs in the I–U curve of the whole generator. The voltage of the global MPP (GMPP), that is, the MPP with the highest power, may fluctuate over a very wide voltage range.[2] The MPPs with lower power are called local MPPs.

PV generators are typically oversized with respect to their connecting inverters, meaning that the generator rated DC power exceeds the inverter rated AC power.[3] Oversizing of a PV generator restricts the generator power to the inverter rated power during high irradiance conditions that occur typically on midday. If the PV generator power production exceeds the maximum power of the inverter, the inverter will limit the PV power by moving the operating point toward higher voltages to limit the produced PV current and power. During these periods the PV generator is not operating at its GMPP. Thus, inverter sizing has a vital effect on the actual operating point of PV generators. Clipping of highest PV powers leads to energy losses. The higher is the DC/AC power ratio, that is, the ratio of the rated PV generator DC power the to the rated inverter AC power, the more energy is lost. PV power variations occurring when the inverter is limiting the PV power are not transmitted to AC power.

Oversizing of PV inverters is common since it reduces relative inverter costs, reduces high power losses of inverters at low power levels, and leads to more constant power production during the day (higher energy production in the morning and afternoon). Low PV module prices and time-of-usage electricity prices, that is, cheaper electricity on midday, motivate to stronger oversizing. The optimal inverter sizing depends on many factors, such as inverter characteristics and irradiance conditions.[4] It is recommended by Zhu et al.[5] that the DC/AC ratio should be from 1.1 to 1.7. However, it was found that the DC/AC ratio should be less than 1 to avoid all power curtailment.[6,7] If the aim is to minimize energy losses, the expected maximum clear-sky irradiance should be the basis for inverter sizing so that the PV generator would be in power-limiting mode only during cloud enhancement.[2] Cloud enhancement is a phenomenon where, under certain conditions, partly cloudy skies have a higher solar irradiance than clear skies due to photons scattering off clouds near the direct path of sunbeams.[6]

Overpassing cloud shadows, which are the main reason for output power variations of large-scale PV systems,[1] cause fast variations in power for PV power plants of all sizes. For example, power variations of over $40\%\,\mathrm{s}^{-1}$ and up to $3\%\,\mathrm{s}^{-1}$ were

K. Lappalainen
Electrical Engineering Unit
Tampere University
33720 Tampere, Finland
E-mail: kari.lappalainen@tuni.fi

The ORCID identification number(s) for the author(s) of this article can be found under https://doi.org/10.1002/aesr.202400199.

DOI: 10.1002/aesr.202400199

measured for a 3.2 kWp PV string[8] and for a 48 MW PV power plant,[9] respectively. Due to the highly variable nature of PV power production, limits have been set for power ramp rates (RR) of grid-connected PV power plants.[10] Compliance with these RR requirements is typically achieved by power output curtailment or using energy storage systems (ESS). However, the use of power curtailment is limited to upward power ramps. Thus, the need for use of ESSs to smooth fluctuating PV production is increasing with strongly increasing installed PV capacity. Several ESS control methods have been proposed in recent years for PV power smoothing.[11] The control method used greatly affects the lifetime, sizing, and price of the ESS, which are tightly linked.[10,12] ESS control methods for power smoothing can be divided into moving average and exponential smoothing-based methods, filter-based methods, RR-based methods, and model predictive control methods.[11,13] DC- and AC-connected energy storage systems for PV power smoothing were compared in.[14] If an ESS is connected in the DC side of the inverter, it allows to store energy that would otherwise be lost due to inverter power curtailment during peak production hours. The effects of the PV system operating point on the operation of PV systems equipped with energy storage have not been studied earlier.

Effective MPP tracking (MPPT) is straightforward and relatively easy to implement under uniform operating conditions. However, during fast output power variations, MPPT may have a delay in following the global MPP, or it can even end up operating in a local MPP instead of the global one.[15,16] Thus, operation of MPPT affects the output power and ESS usage of PV systems. MPP characteristics of PV generators have been studied by simulations in[15,17–20] and based on electrical measurements in.[2,8,21] However, the effects of inverter sizing on the operating point are considered only in.[2,21] Moreover, static and unrealistic shading patterns were used in some studies such as.[18] Several MPPT algorithms have been developed during the last years.[22,23] Sangwongwanich et al. proposed an MPPT-based power smoothing method which reduces the rate of change in power by moving the operating point away from the MPP.[24]

Since highly varying GMPP voltage causes large fluctuation of the inverter reference voltage, posing challenges for MPPT, it would be beneficial to keep the operating point of the inverter all the time at voltages close to the nominal MPP voltage.[2,8] In this way, the operation of the PV system would be more straightforward, smoother, and more predictable. The wide operating voltage range of the GMPP can be significantly reduced by operating at the MPP closest to the nominal MPP voltage (CMPP) at a cost of minor energy losses.[2] However, the fastest power variations of the CMPP are faster than those of the GMPP.[8] The characteristics of the CMPP and differences between the GMPP and CMPP have been studied in.[2,8,21]

In this article, effects of the operating point on the operation of PV systems equipped with ESSs are studied for the first time. The aim of this study is to find out how keeping the operating point of a PV inverter all the time at voltages close to the nominal MPP voltage instead of the GMPP affects the sizing and usage of the ESS used for PV power smoothing. DC- and AC-connected ESSs are compared. The study is based on a wide set of measured *I*–*U* curves of a 23 module PV string. Use of the measured *I*–*U* curves instead of AC powers allows studying the technology-independent ESS requirements imposed by PV power variability without taking into account the nonidealities and losses related to MPPT, inverter, etc. In that way, the results are not as tied to a certain system. For the same reason, losses of the ESS were not considered. Moreover, the use of the measured *I*–*U* curves allows easy simulation of various DC/AC power ratios and to compare DC and AC ESS connection topologies.

The rest of this article is organized as follows. In Section 2.1, the measurement data used is introduced. Section 2.2 introduces the energy storage control strategy used and illustrates its operation. The results of the study are presented in Section 3 and they are further discussed in Section 4. Finally, the conclusions of the article are provided in Section 5.

2. Experimental Section

2.1. Data

The experimental data consists of *I*–*U* curves of a 23 module PV string measured in May, June, July, August, and September 2023 in the PV power research plant of Tampere University.[25] In total, 32 days of full-time measurements were analyzed. Measurement period of each day was 12 h: from 7:00 to 19:00 (UTC + 2). The period was selected so that all hours with considerable daylight were included in the analysis. An *I*–*U* curve consisting of 4000 measurement points was measured once a second during the measurement period, using an *I*–*U* curve tracer where parallel-connected IGBTs act as a variable load. Thus, in total, 1 382 400 measured *I*–*U* curves were analyzed. *I*–*U* curves were measured from open-circuit (OC) to short-circuit (SC). The current and voltage were measured by a Tektronix TCP312A current probe with a Tektronix TCPA300 current probe amplifier and a LeCroy AP031 differential voltage probe, respectively. Each measured *I*–*U* curve was preprocessed by the following procedure. First, the measurement points with identical voltage value were replaced with a single point by averaging their current values. After that, clearly abnormal measurement points were eliminated. A point was eliminated if its power differed from the power of the previous and next point by more than 1.3 times the mean power change between previous and next 9 points. Finally, the current and voltage values of each measured curve were smoothed separately using the smooth.m function in MATLAB. **Figure 1** shows a measured power–voltage curve near the GMPP illustrating the preprocessing procedure.

Nine PV modules of the string have been equipped with irradiance and temperature measurements with a sampling frequency of 10 Hz. The irradiance incident on the PV modules was measured by photodiode-based SP Lite2 pyranometers mounted at the same 157° azimuth angle from north to east and 45° tilt angle as the PV modules. The back-sheet temperature of the modules was measured by Pt100 temperature sensors. The layout of the studied PV string is presented in **Figure 2**.

The nominal standard test conditions (STC) values of the studied string at the MPP, OC, and SC are compiled in **Table 1**. The PV string is composed of 23 NAPS NP190GK modules. Each module consists of 3 submodules of 18 polycrystalline silicon PV cells protected by an antiparallel-connected bypass diode.

Figure 3 shows the distributions of the measured average irradiances and temperatures of the studied PV string during the

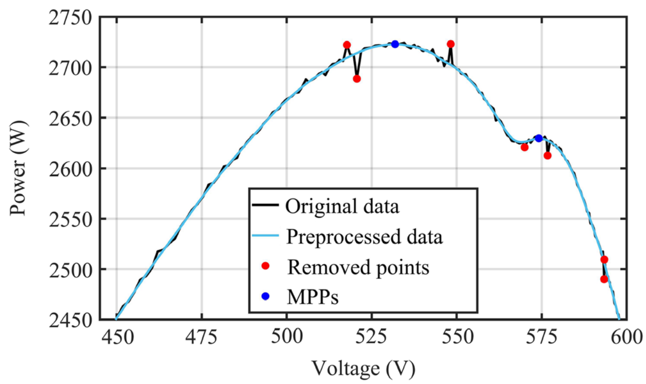

Figure 1. Original and preprocessed power–voltage curve near the GMPP.

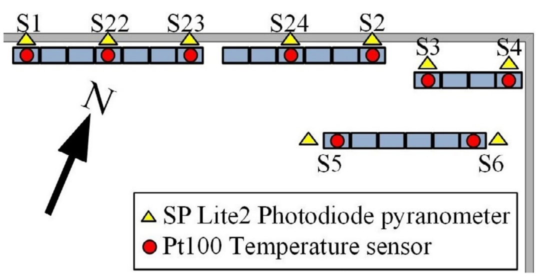

Figure 2. Layout scheme of the studied PV string indicating the locations of the PV modules and their irradiance and temperature sensors.

Table 1. Electrical parameter values of the studied string.

$P_{MPP, STC}$ [W]	$U_{MPP, STC}$ [V]	$I_{MPP, STC}$ [A]	$U_{OC, STC}$ [V]	$I_{SC, STC}$ [A]
4370	593	7.36	759	8.00

measurement period of 32 days. The irradiance distribution has clearly two peaks: one around 100 W m^{-2} formed by low irradiance levels in mornings and evenings and during overcast periods and another one around 850 W m^{-2} corresponding to clear-sky conditions around noon. The temperature of the PV modules was most of the time quite low: temperatures from 20 to 30 °C were most common while below 15 °C or above 60 °C temperatures were rare.

The relative cumulative frequency of the measured irradiance difference within the PV string is presented in **Figure 4**. The distribution shows that irradiance differences lower than 125 W m^{-2} or so were quite typical while higher differences were quite infrequent. The difference between the highest and lowest irradiance measurement of the string was 30.3%, 4.8%, and 3.4% of the time over 100, 200, and 400 W m^{-2}, respectively. The highest measured irradiance difference was 726 W m^{-2}. All measured PV module temperatures of the string were 69% of the time within 5 °C from each other while the highest measured difference in temperature was 29 °C.

Daily average irradiances and shares of time when the string was partially shaded are compiled in **Table 2**. There was a great variation in irradiance conditions between the days. Most of the

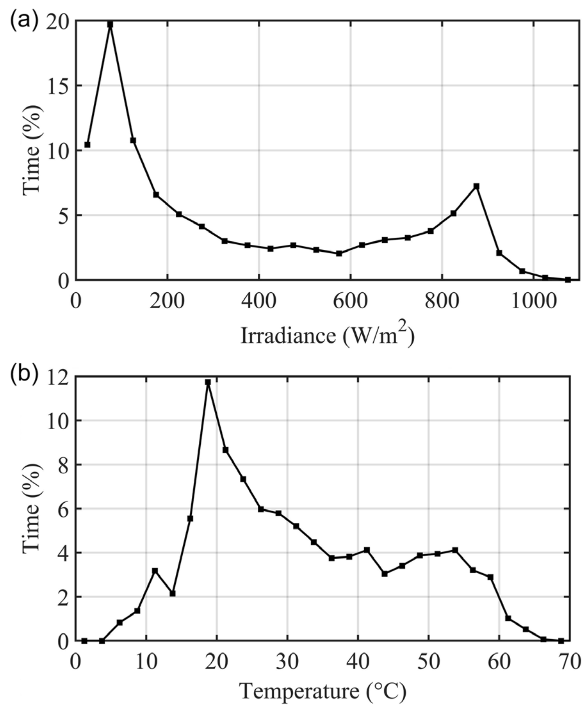

Figure 3. Distributions of the average a) irradiances and b) temperatures of the PV string calculated as the average of all the nine measurements of the string.

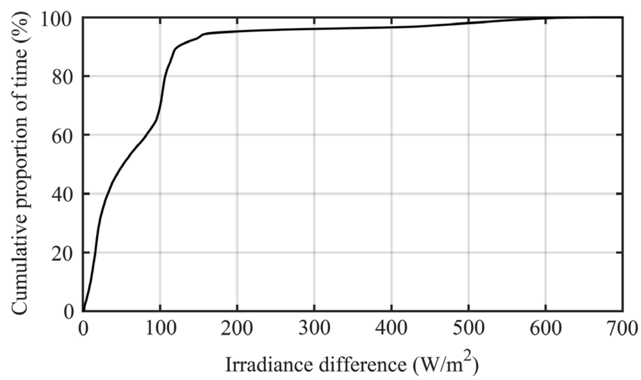

Figure 4. Relative cumulative frequency of the difference between the highest and lowest irradiance measurement of the string.

days had clear-sky conditions, at least periodically, but there were also a few fully overcast days. The highest daily average irradiance was nearly 600 W m^{-2} while the average irradiance in fully overcast days was less than 100 W m^{-2}. On average, the daily average irradiance was about 350 W m^{-2}. The daily share of time when irradiance difference within the string was more than 100 W m^{-2} varied from 0% to 61%. The corresponding range for an irradiance difference of more than 200 W m^{-2} was from 0% to 11%.

2.2. Energy Storage Control Strategy

PV power smoothing was implemented by a virtual ESS controlled with an RR-based control strategy where the RR of the

Table 2. Daily average irradiances and shares of time when the studied PV string was partially shaded so that the difference between the lowest and highest irradiance measurement exceeded 100 and 200 W m^{-2}. The average irradiances are calculated as the average of all the nine measurements of the string.

Date	Average irradiance [W m^{-2}]	100 W m^{-2} partial shading [%]	200 W m^{-2} partial shading [%]
May 22, 2023	449	42.00	6.18
May 23, 2023	378	27.95	2.34
May 24, 2023	534	61.07	9.02
May 25, 2023	362	31.63	1.13
May 26, 2023	147	5.83	0.96
May 27, 2023	504	53.37	10.45
May 28, 2023	163	5.91	0.30
June 12, 2023	581	57.84	8.23
June 13, 2023	565	51.38	8.22
June 14, 2023	537	44.74	8.20
June 15, 2023	546	49.01	8.21
June 16, 2023	544	46.66	8.22
June 17, 2023	411	26.83	1.50
June 18, 2023	546	43.90	8.25
June 19, 2023	561	44.06	8.28
June 20, 2023	484	41.37	8.41
June 21, 2023	529	41.35	8.64
June 22, 2023	100	2.07	1.59
June 23, 2023	544	52.06	9.37
June 24, 2023	271	12.71	2.72
June 25, 2023	393	45.02	10.10
July 31, 2023	94	0.00	0.00
August 1, 2023	128	2.15	1.22
August 2, 2023	96	0.08	0.00
August 3, 2023	255	15.34	2.06
September 11, 2023	49	0.00	0.00
September 12, 2023	278	23.48	1.30
September 13, 2023	111	0.97	0.06
September 14, 2023	438	59.16	11.18
September 15, 2023	417	53.53	6.01
September 16, 2023	159	6.67	0.43
September 17, 2023	210	20.38	1.97
Average	356	30.27	4.83
Standard deviation	180	21.23	3.95

power fed to the grid P_{grid} was limited to comply with the applied RR limit (RRL). DC and AC ESS connection topologies were compared. **Figure 5** shows the simulation models used, containing the PV string, the ESS and an inverter. Losses in the inverter and cables were not taken into account. Thus, the DC power of the inverter $P_{inv,\ DC}$ was equal to the AC power of the inverter $P_{inv,\ AC}$. In the DC connection topology, the generated PV power P_{PV} equals the sum of P_{grid} and the charging power of the ESS

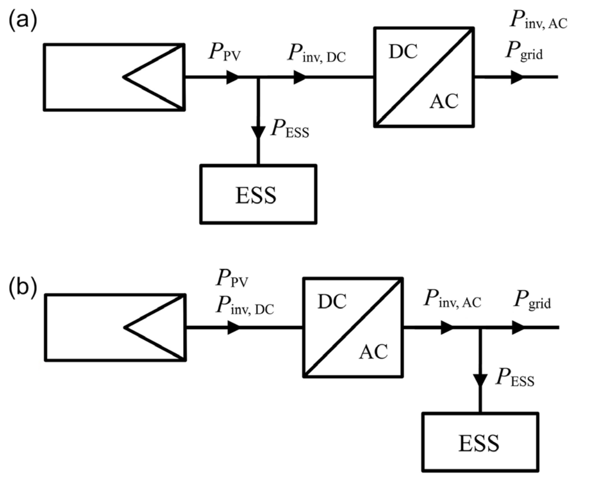

Figure 5. Diagrams of the PV system simulation model with a) a DC-connected ESS and b) an AC-connected ESS.

P_{ESS}, that is, $P_{PV} = P_{grid} + P_{ESS}$. In the case of an AC-connected ESS, $P_{inv,\ AC}$ equals the sum of P_{grid} and P_{ESS}, that is, $P_{inv,\ AC} = P_{grid} + P_{ESS}$. Positive P_{ESS} corresponds to charging and negative to discharging of the ESS.

In order to ensure RRL compliance at any time, even during a sudden shutdown of the PV system, enough energy is stored in the ESS all the time to lower P_{grid} to zero with the applied RRL. Thus, the minimum energy stored in the ESS at each moment can be defined as

$$E_{ESS,\min} = \frac{{P_{grid}}^2}{2\mathrm{RRL}}. \tag{1}$$

The ESS energy level was kept as close to the minimum as possible by discharging the ESS whenever possible. Thus, the ESS control strategy smooths the power fed to the grid mainly based on the minimum energy requirement of Equation (1). Keeping the ESS as empty as possible limits the power fed to the grid more than an RR limitation based purely on the RR of P_{grid}. This ESS control strategy was selected as it minimizes the required ESS energy capacity. RRLs of 1, 5, 10, and 20% min^{-1} with respect to the nominal MPP power of the PV string were used.

The effects of inverter sizing on the operation of PV strings were studied by varying the ratio of the nominal PV DC power to the inverter nominal AC power, that is, the DC/AC ratio. The maximum power fed to the grid $P_{grid,\ max}$ was limited by the inverter sizing and grid connection power which were selected equal. Thus, $P_{grid,\ max}$ is defined by the DC/AC ratio as

$$P_{grid,\max} = \frac{P_{PV,\,nom}}{\mathrm{DC/AC\ ratio}} \tag{2}$$

where $P_{PV,\ nom}$ is the nominal PV power, that is, the PV string $P_{MPP,\ STC}$ listed in Table 1. MPPT of the PV string was assumed to be ideal, meaning that the string is operating at the GMPP (or the CMPP) unless it is in power-limiting mode. If the power at the GMPP (or the CMPP) is higher than the nominal power of the inverter, the string operates on the high voltage side of

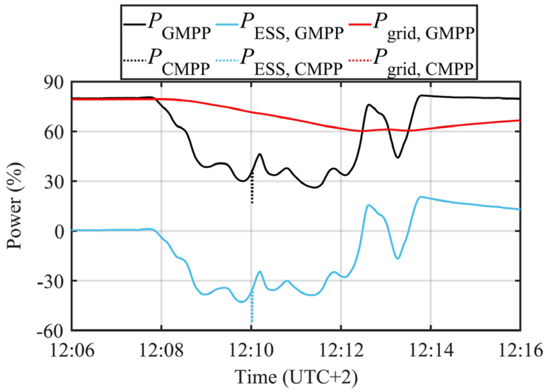

Figure 6. PV string GMPP and CMPP powers, the powers fed to the grid and the powers of the DC-connected ESS with an RR limit of 10% min^{-1} on June 17, 2023. The powers are with respect to the PV string nominal MPP power. The curves for the powers fed to the grid are overlapping each other.

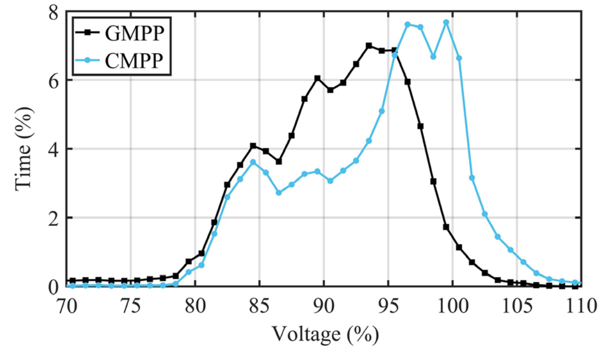

Figure 7. Distributions of the measured GMPP and CMPP voltages. The voltages are with respect to the PV string nominal MPP voltage.

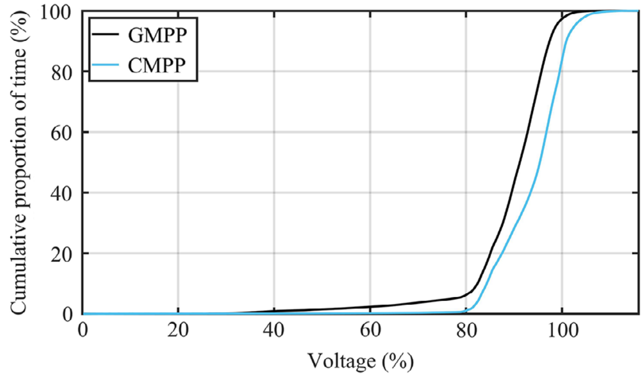

Figure 8. Relative cumulative frequencies of the measured GMPP and CMPP voltages. The voltages are with respect to the PV string nominal MPP voltage.

the GMPP (or the CMPP) at the lowest voltage where the nominal power of the inverter is not exceeded. The DC/AC ratio was varied from 0.8 to 2.0.

Figure 6 illustrates operation of the ESS control strategy showing the measured GMPP and CMPP powers together with the corresponding powers of a DC-connected ESS and the powers fed to the grid for a period of 10 min. After the generated PV power starts to decrease around 12:08, the ESS smooths the power fed to the grid. However, the power fed to the grid decreases slower than the applied RR limit of 10% min^{-1} allows. The reason for this is that the ESS is kept as empty as possible, that is, as much energy is discharged from the ESS to the grid as possible. A difference between operation at the GMPP and at the GMPP is visible around 12:10 when there is momentarily a local MPP closer to the nominal MPP voltage than the GMPP. At this moment, the CMPP power decreases for a moment and that decrease is compensated by taking more power from the ESS. However, this has only a negligible effect on the power fed to the grid.

3. Results

3.1. PV Strings without Energy Storage

Figure 7 shows the distributions of the measured GMPP and CMPP voltages. Voltages of both operating points were most of the time below the STC MPP voltage. This results from the operating conditions of the string (see Figure 3): average irradiance was, most of the time, lower and average temperature higher than in STC. There is a clear difference between the operating points. Voltage of the CMPP was more often close to the STC MPP voltage and more seldom below 96% with respect to the STC MPP voltage compared to the GMPP. In particular, the CMPP voltage was much more seldom between 85% and 95% or so with respect to the STC MPP voltage than the GMPP voltage. These results are line with earlier findings.[2]

Figure 8 shows the relative cumulative frequencies of the measured GMPP and CMPP voltages. Figure 8 reveals that the GMPP voltage was much more often from 40% to 80% of the nominal MPP voltage than the CMPP voltage. The GMPP voltage was 6.3% of the time below 80% while the corresponding share was only 1.1% for the CMPP voltage. The highest measured voltages of the two MPPs were quite close to each other: 113.5% and 115.9% for the GMPP and CMPP, respectively. These results mean that, in practice, the CMPP has drastically narrower voltage range than the GMPP. The CMPP voltage was 71.6% and 98.9% of the time within 10% and 20% of the nominal MPP voltage. The corresponding shares for the GMPP were 56.9% and 93.7%. Moreover, the fastest voltage fluctuations of the CMPP were much lower than those of the GMPP. These results indicate that MPPT is expected to meet less difficulties when trying to follow the CMPP instead of the GMPP.

The CMPP differs from the GMPP when the operating conditions of the PV string are uneven which is typically caused by partial shading. This was most frequent during mornings and evenings when PV power production is low. The distributions of the measured GMPP and CMPP powers are presented in **Figure 9**. There were only minor differences between the operating points: powers below 15% with respect to the nominal MPP power were somewhat more common for the CMPP while the GMPP power was slightly more often between 20% and 50% or so. Indeed, there are much smaller differences between the two MPPs in power than in voltage which can be seen by

ADVANCED ENERGY & SUSTAINABILITY RESEARCH
www.advenergysustres.com

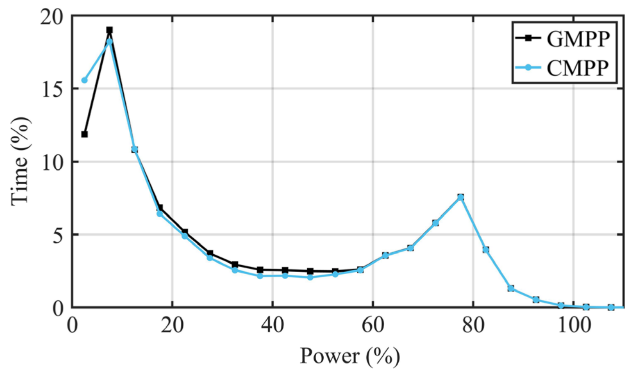

Figure 9. Distributions of the measured GMPP and CMPP powers. The powers are with respect to the PV string nominal MPP power.

comparing Figure 7 and 9. The reason for this is that typically when a PV system is having multiple MPPs due to partial shading, the power is quite even over a wide voltage range.[8] Thus, there can be large voltage differences between the two operating points while they have only minor differences in power. Even smaller differences in power distributions between the GMPP and CMPP were reported earlier.[2]

Small power differences between the two operating points supports operation at the CMPP instead of the GMPP. The extremely wide operating voltage range can be shrunk considerably without causing significant energy losses. However, following the CMPP is more challenging in some cases as the fastest rates of change in power are higher for the CMPP than for the GMPP. An example of very fast CMPP power fluctuation is visible in Figure 6 around 12:10.

Figure 10 shows the relative energy losses due to operation at the CMPP instead of the GMPP as a function of the DC/AC ratio. The losses were almost constant, around 3.0% with respect to energy produced at the GMPP, at DC/AC ratios lower than 1.2. At higher DC/AC ratios, the relative losses increased with increasing DC/AC ratio. As the DC/AC ratio increases the share of time when the inverter is limiting the power output increases lowering the absolute energy yield difference between the operating points slightly. However, the relative energy yield difference calculated with respect to energy produced at the GMPP considering power curtailment increases with increasing DC/AC ratio as the energy produced at the GMPP decreases strongly due to power curtailment.

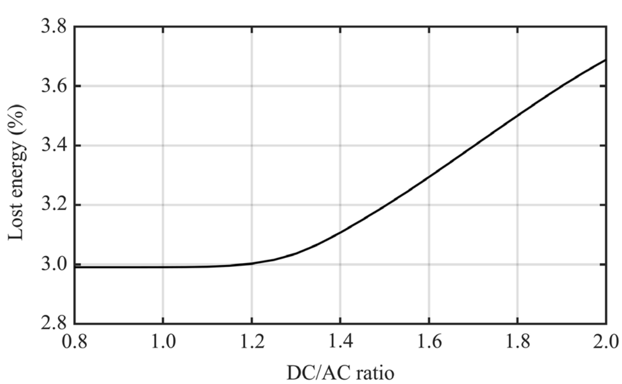

Figure 10. Relative energy losses due to operation at the CMPP instead of the GMPP as a function of the DC/AC ratio. The losses are with respect to energy produced at the GMPP considering power curtailment.

Daily relative energy losses due to operation at the CMPP instead of the GMPP without considering any power curtailment are compiled in **Table 3**. There were large differences between the days as the operating conditions may differ greatly from day to day. The daily losses varied between 0.2% and 7.6% with respect to energy produced at the GMPP. On average, 2.6% of

Table 3. Daily relative energy losses due to operation at the CMPP instead of the GMPP without considering any power curtailment calculated with respect to energy produced at the GMPP.

Date	Energy losses due to operation at the CMPP instead of the GMPP [%]
May 22, 2023	1.38
May 23, 2023	0.77
May 24, 2023	4.38
May 25, 2023	0.16
May 26, 2023	0.45
May 27, 2023	4.73
May 28, 2023	0.84
June 12, 2023	4.20
June 13, 2023	4.05
June 14, 2023	3.18
June 15, 2023	3.56
June 16, 2023	4.16
June 17, 2023	0.90
June 18, 2023	3.80
June 19, 2023	4.47
June 20, 2023	5.83
June 21, 2023	4.12
June 22, 2023	2.48
June 23, 2023	4.10
June 24, 2023	0.32
June 25, 2023	5.85
July 31, 2023	2.32
August 1, 2023	1.79
August 2, 2023	2.98
August 3, 2023	0.89
September 11, 2023	7.56
September 12, 2023	0.72
September 13, 2023	1.14
September 14, 2023	1.52
September 15, 2023	1.32
September 16, 2023	1.01
September 17, 2023	0.84
Average	2.68
Standard deviation	1.93

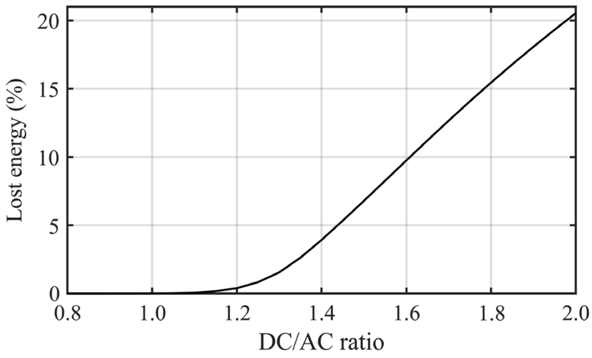

Figure 11. Relative energy losses due to power curtailment as a function of the DC/AC ratio calculated with respect to energy produced at the GMPP without power curtailment.

daily produced energy was lost due to operation at the CMPP instead of the GMPP.

The relative energy losses of the studied PV strings due to power curtailment are shown in **Figure 11** as a function of the DC/AC ratio. At low DC/AC ratios, only minor losses occurred due to power curtailment since the inverter was limiting PV string only seldomly. The theoretical maximum clear-sky irradiance in the Tampere region is around 900 W m^{-2} meaning that with a DC/AC ratio of around 1.1 or lower the PV power exceeds inverter power only during cloud enhancement. At DC/AC ratios higher than 1.2 or so, the relative energy losses due to power curtailment increased strongly with increasing DC/AC ratio. With a DC/AC ratio of 2.0 over 20% of the available PV energy was lost due to power curtailment. This means that a DC- connected ESS has a huge potential for improving the energy yield of a PV system with a strongly undersized inverter compared to an AC-connected ESS.

3.2. PV Strings with Energy Storage

Figure 12 shows the required charging and discharging power capacities for a DC-connected ESS as a function of the DC/AC ratio. In general, the ESS charging power requirement increases with decreasing RRL since the stricter is the RRL the more ESS charging power is needed to comply with the limit during fast upward irradiance transitions. The operating point had only a minor difference on the ESS charging power requirement. There were some small differences with the loosest RRL studied but in other cases the curves of the GMPP and CMPP are overlapping each other. In general, the ESS discharging power requirement decreases with increasing DC/AC ratio and the RRL does not have a significant effect on it. There was a clear difference between the GMPP and CMPP in the ESS discharging power requirement. The required ESS discharging power was higher if the PV string operated at the CMPP instead of the GMPP. This results from fast CMPP power fluctuations illustrated in Figure 6 occurring when there is momentarily a local MPP closer to the nominal MPP voltage than the GMPP. The difference between the operating points decreased with increasing DC/AC ratio as the time when the system is in power-limiting mode, that is, not operating at the specific MPP

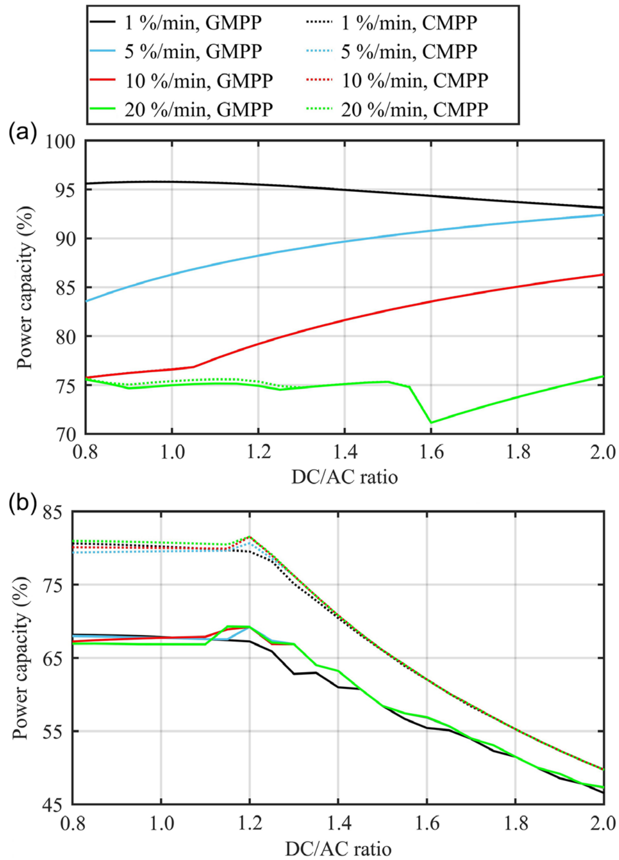

Figure 12. Required a) charging and b) discharging power capacities for a DC- connected ESS as a function of the DC/AC ratio for several RRLs. The capacities are with respect to the PV string nominal MPP power.

increased. The results show that the charging power requirement of a DC-connected ESS is higher than the discharging power requirement if the PV system operates at its GMPP. This finding is in line with earlier results.[26] The reason for it is that ESS charging compensates PV power increases also when the inverter size is limiting the power fed to the grid while the ESS discharge always starts from the power fed to the grid. If the PV system operates at the CMPP, the charging power requirement of a DC-connected ESS is higher than the discharging power requirement except with the combination of a loose RRL and a low DC/AC ratio.

The required charging and discharging power capacities for an AC-connected ESS are presented in **Figure 13** as a function of the DC/AC ratio. Both requirements decreased strongly with increasing DC/AC ratio. This is an expected result as the AC power is the smoother the higher is the DC/AC ratio. The RRL had a relatively small effect on the power requirements for an AC-connected ESS. The operating point had only minor effects on the required charging power existing mainly at DC/AC ratios higher than 1.6. On the contrary, the required ESS discharging power is clearly higher for the CMPP than for the GMPP at all DC/AC ratios. This results from the aforementioned fast CMPP power fluctuations that are typically transmitted to AC power. Comparison between Figure 12 and 13 reveals that an

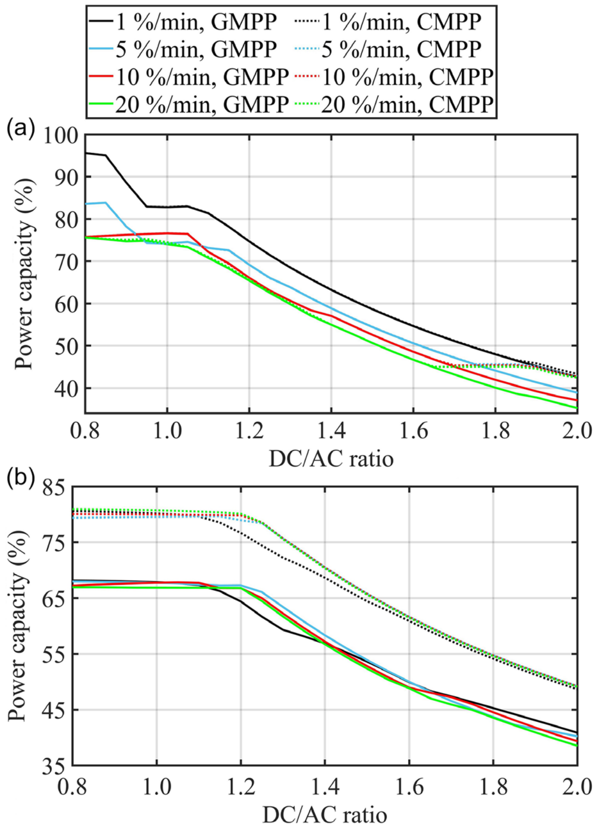

Figure 13. Required a) charging and b) discharging power capacities for an AC- connected ESS as a function of the DC/AC ratio for several RRLs. The capacities are with respect to the PV string nominal MPP power.

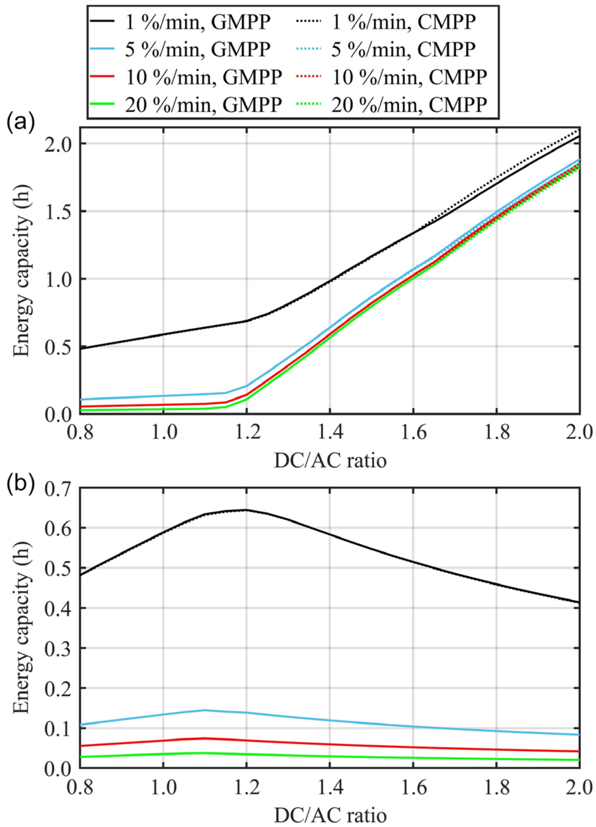

Figure 14. Required energy capacities for a) a DC-connected ESS and b) an AC-connected ESS as a function of the DC/AC ratio for several RRLs. The capacities are with respect to the PV string nominal MPP power.

AC-connected ESS has lower ESS charging and discharging power requirements than a DC-connected ESS. Especially the required charging power capacities at high DC/AC ratios were clearly lower for AC-connected ESSs.

Figure 14 shows the energy capacity requirements for a DC-connected ESS and an AC- connected ESS as a function of the DC/AC ratio. The energy capacity requirements increased with tightening RRL as the need for power smoothing increased. The required energy capacity for a DC-connected ESS increased with increasing DC/AC ratio since the clipped energy was stored in the ESS. The AC ESS energy capacity requirement was much more independent of the DC/AC ratio being the highest at DC/AC ratios of roughly 1.1. Differences in energy capacity requirements between the GMPP and CMPP were small. The largest differences existed in the requirements for a DC-connected ESS at high DC/AC ratios: the energy capacity requirement was higher for the CMPP when an RRL of 1% min^{-1} was applied. With other RRLs studied the requirement was higher for the GMPP. The energy capacity requirements for a DC-connected ESS and an AC-connected ESS were close to each other at low DC/AC ratios as the powers to be smoothed were almost similar due to low power curtailment. The higher the DC/AC ratio, the more the AC power was clipped and the higher the difference in energy capacity requirements between the DC- and AC-connected ESSs. The results obtained for the GMPP with a DC-connected ESS are in accord with earlier results.[26]

The results of Figure 12 and 13 show that following the CMPP instead of the GMPP increases the requirement for ESS discharging power capacity especially at low DC/AC ratios. However, the ESS charging power requirement of a DC-connected ESS was found to be higher than the discharging power requirement except for the CMPP at the lowest DC/AC ratios studied. Typically, the charging power rating of an ESS equals to its discharging power rating. In that case and with typical DC/AC ratios of around 1.5, the practical meaning of the differences between the MPPs is marginal for PV systems equipped with a DC-connected ESS. Moreover, Figure 14 shows that there were only minor differences in ESS energy capacity requirements between the GMPP and CMPP. Thus, these results mean that, in practice, there are no major differences in sizing of DC-connected ESSs between these two MPPs.

Daily power and energy capacity requirements for a DC-connected ESS and an AC-connected ESS are listed in **Table 4** and **5** for an RR limit of 10% min^{-1} and a DC/AC ratio of 1.5. There were large differences between the days, due to differences in daily operating conditions, especially in the required ESS energy capacity. The required energy capacity varied from 0.001 h to 0.82 h with respect to the PV string nominal MPP power for the DC-connected ESS and from 0.001 to 0.056 h

Table 4. Daily power and energy capacity requirements for a DC-connected ESS for an RR limit of 10% min^{-1} and a DC/AC ratio of 1.5 for all the 32 days. The capacities are with respect to the PV string nominal MPP power.

Date	Required power capacity [%], GMPP	Required energy capacity [h], GMPP	Required power capacity [%], CMPP	Required energy capacity [h], CMPP
May 22, 2023	50.3	0.152	66.0	0.149
May 23, 2023	60.4	0.263	65.8	0.259
May 24, 2023	56.9	0.549	65.6	0.544
May 25, 2023	55.7	0.322	59.9	0.322
May 26, 2023	58.5	0.048	58.5	0.047
May 27, 2023	52.6	0.821	64.9	0.819
May 28, 2023	28.6	0.039	28.6	0.039
June 12, 2023	53.4	0.755	62.8	0.749
June 13, 2023	47.1	0.597	65.4	0.591
June 14, 2023	29.5	0.343	66.0	0.339
June 15, 2023	31.2	0.374	65.4	0.369
June 16, 2023	28.9	0.344	65.7	0.339
June 17, 2023	52.2	0.096	65.4	0.095
June 18, 2023	36.8	0.441	61.6	0.436
June 19, 2023	40.0	0.494	65.7	0.488
June 20, 2023	57.6	0.395	66.0	0.392
June 21, 2023	53.6	0.360	66.0	0.356
June 22, 2023	7.8	0.007	6.9	0.006
June 23, 2023	58.5	0.589	65.8	0.583
June 24, 2023	82.6	0.061	82.6	0.061
June 25, 2023	61.9	0.285	66.0	0.283
July 31, 2023	6.4	0.007	9.3	0.007
August 1, 2023	43.0	0.025	44.0	0.025
August 2, 2023	31.0	0.017	31.1	0.017
August 3, 2023	49.3	0.063	61.5	0.063
September 11, 2023	1.2	0.001	3.3	0.001
September 12, 2023	62.0	0.092	62.1	0.091
September 13, 2023	66.2	0.024	66.2	0.024
September 14, 2023	55.3	0.161	65.3	0.160
September 15, 2023	71.1	0.205	71.2	0.205
September 16, 2023	66.7	0.043	66.7	0.043
September 17, 2023	71.7	0.098	71.7	0.098
Average	47.7	0.252	57.3	0.250
Standard deviation	19.3	0.234	19.5	0.232

Table 5. Daily power and energy capacity requirements for an RR limit of 10% min^{-1} and a DC/AC ratio of 1.5 for all the 32 days. The capacities are with respect to the PV string nominal MPP power.

Date	Required power capacity [%], GMPP	Required energy capacity [h], GMPP	Required power capacity [%], CMPP	Required energy capacity [h], CMPP
May 22, 2023	42.7	0.055	63.2	0.055
May 23, 2023	48.4	0.056	65.1	0.056
May 24, 2023	47.9	0.056	65.0	0.056
May 25, 2023	45.0	0.056	53.9	0.056
May 26, 2023	35.5	0.036	35.5	0.036
May 27, 2023	50.0	0.056	62.1	0.056
May 28, 2023	28.6	0.039	28.6	0.039
June 12, 2023	5.8	0.056	62.5	0.056
June 13, 2023	13.3	0.056	65.1	0.056
June 14, 2023	4.3	0.056	65.8	0.056
June 15, 2023	4.6	0.056	65.2	0.056
June 16, 2023	17.6	0.056	64.9	0.056
June 17, 2023	47.2	0.055	59.3	0.055
June 18, 2023	5.2	0.056	59.8	0.056
June 19, 2023	5.7	0.056	65.5	0.056
June 20, 2023	47.7	0.056	62.6	0.056
June 21, 2023	44.1	0.056	62.0	0.056
June 22, 2023	7.8	0.007	6.9	0.006
June 23, 2023	50.6	0.056	63.8	0.056
June 24, 2023	45.2	0.042	45.2	0.042
June 25, 2023	52.8	0.056	60.2	0.056
July 31, 2023	6.4	0.007	9.3	0.007
August 1, 2023	43.0	0.025	40.6	0.025
August 2, 2023	31.0	0.017	31.1	0.017
August 3, 2023	33.7	0.048	55.8	0.048
September 11, 2023	1.2	0.001	3.3	0.001
September 12, 2023	40.5	0.055	45.9	0.054
September 13, 2023	38.2	0.021	38.2	0.021
September 14, 2023	46.8	0.056	53.0	0.056
September 15, 2023	49.4	0.055	58.4	0.055
September 16, 2023	49.1	0.037	49.1	0.037
September 17, 2023	52.6	0.054	52.6	0.053
Average	32.5	0.045	50.6	0.045
Standard deviation	18.5	0.017	18.0	0.017

for the AC-connected ESS. The variation in required power capacity was the largest for the DC-connected ESS when the GMPP was followed. Large daily variation in power capacity requirements for the GMPP with a DC-connected ESS is in line with earlier results.[26] Comparison between Table 4 and 5 and Table 2 discloses that the ESS power and energy requirements were the lowest on fully overcast days. On those days, irradiance level was low and no fast irradiance fluctuations occurred meaning that there was only a minor need for power smoothing. Standard deviations of the ESS requirements reveal that there was relatively much higher variation between the days in the energy requirements than in the power requirements. The power requirements were higher and energy requirements slightly lower for the CMPP than for the GMPP in line with Figure 12–14.

Shares of produced PV energy that was cycled through the ESS are presented in **Figure 15** as a function of the DC/AC ratio. The

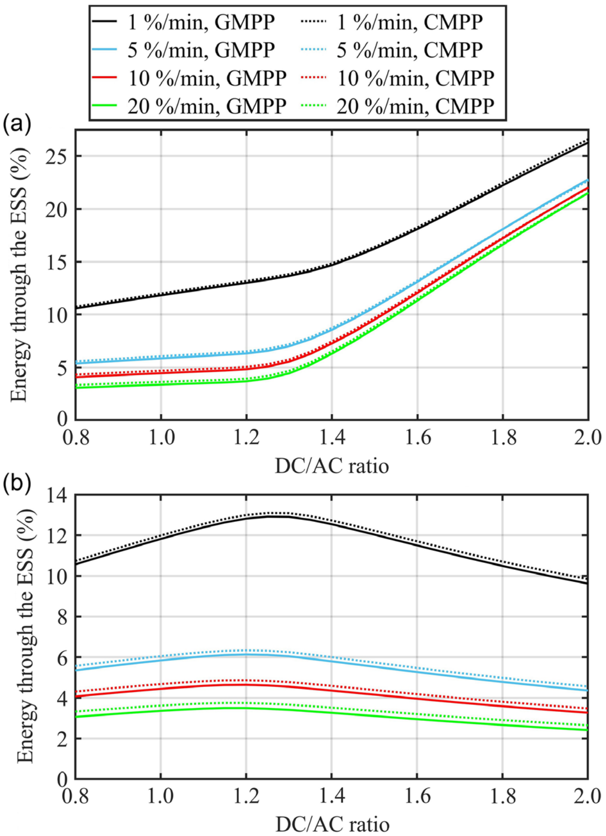

Figure 15. Shares of produced PV energy cycled through a) a DC-connected ESS and b) an AC-connected ESS as a function of the DC/AC ratio for several RRLs.

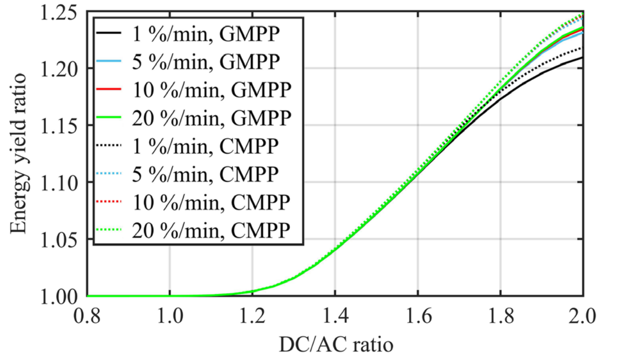

Figure 16. Energy yield ratio as a function of the DC/AC ratio for several RRLs.

shape of the curves is quite similar than those of required energy capacities in Figure 14. The shares of energy cycled through the ESS increased as the RRL decreased since a lower RRL means a higher need for power smoothing. At low DC/AC ratios, there were only negligible differences between the DC- and AC-connected ESSs since only minor power curtailment existed. Shares of energy cycled through a DC-connected ESS increased with increasing DC/AC ratio since the clipped energy was cycled through the ESS. The shares of energy cycled through the ESS were slightly higher when the CMPP was followed instead of the GMPP. The results obtained for the GMPP with a DC-connected ESS are in line with earlier results.[26] There was large variation in daily shares of energy cycled through the ESS. It varied from about 2% to about 18% and from about 1% to about 13% for the DC- and AC-connected ESSs, respectively, in the case of an RR limit of 10% min^{-1} and a DC/AC ratio of 1.5. The ranges were somewhat larger for the GMPP than for the CMPP. The shares of energy cycled through the ESS were the lowest on overcast days with a minor need for power smoothing.

Figure 16 shows the energy yield ratio, that is, the ratio of the total energy fed to the grid when a DC-connected ESS is used to the total energy fed to the grid when an AC-connected ESS is used, as a function of the DC/AC ratio. The energy yield ratio was close to one at low DC/AC ratios meaning that almost the same amount energy was fed to the grid regardless of the connection point of the ESS. The energy yield ratio increased strongly with increasing DC/AC ratio at ratios higher than 1.2. With a DC/AC ratio of 2.0, the DC-connected ESS allowed to feed from 21% to 25% more energy to the grid than the AC-connected ESS. These results are in accord with earlier results.[14] The energy yield ratios increased with increasing RRL and were somewhat higher for the CMPP than for the GMPP. The results mean that if an ESS is used for PV power smoothing the total energy fed to the grid can be considerable increased by connecting the ESS to the DC bus of the inverter instead of the AC bus. On the contrary, a DC- connected ESS has higher ESS power and energy requirements than an AC-connected ESS. There was some variation in the energy yield ratios between the days. It varied from 1.0 to 1.2 for both MPPs with an RR limit of 10% min^{-1} and a DC/AC ratio of 1.5 being somewhat higher for the CMPP than for the GMPP.

4. Discussion

The main objective of this study was to determine how a scenario in which the MPP closest to the nominal MPP voltage is followed instead of the GMPP affects the power and energy requirements that PV power variability imposes on the ESSs used for power smoothing of PV strings. The energy storage control strategy used affects these requirements. In this study, an RR-based control strategy was selected. The main drawbacks of typical moving average and low-pass filter-based control strategies are that they lead to unnecessary ESS usage during small power variations.[13] Moreover, the control strategy selected minimizes the required ESS energy capacity by keeping the ESS as empty as possible all the time. Comparison between various control strategies would be an interesting topic for future studies.

The measurement period and the location where the measurements were performed affected the obtained results. As can be seen from Table 3, the daily operating conditions have a crucial effect on the differences between the two MPPs. Different distributions of operating conditions (Figure 3) and operating point characteristics (Figure 7 and 9) would have been obtained if the measurements were performed at different times of year. The results show that the power and energy requirements that PV power variability imposes on the ESSs are the lowest on fully overcast days with a minor need for power smoothing. Fully overcast days are most frequent during winter and late-fall. In order to minimize the effects of weighting of different day types (clear sky, overcast, etc.) on the results, all kinds of days were included in the study and the most important results were presented as daily values. This allowed to illustrate the daily ranges of variation and enhanced the applicability of the results to different locations. The measurements were performed near midsummer when the irradiance levels and PV production are typically the highest. This selection increased the applicability of the results to locations with better irradiance conditions. It was found in[1] that there are no clear trends in monthly amounts or other features of irradiance transitions caused by overpassing cloud shadows in the Tampere region during the summer period from April to September. Moreover, there are differences between years. Thus, measurement data of several years would have been optimal to provide highly reliable results. However, that kind of dataset was not available. The measurements were performed in Tampere, Finland and the measurement system was located on the rooftop of a campus building where shadings by nearby built structures occur occasionally. Thus, the exact values are representative of mainly PV systems installed in built environments on high-latitude locations. However, the general observations of the studied phenomena and the conclusions drawn from the results can be applied globally. Validation of the results in different geographical locations and under different climatic conditions is an interesting topic for future research.

In this study, MPPT was assumed to be ideal, meaning that the PV string was operating at the selected MPP constantly unless it was in power-limiting mode. However, ideal MPPT is not possible in practice. Especially, the fast variations of GMPP voltage over a wide range could lead to periods when the PV system is operating in a local MPP or is not operating at any MPP. Moreover, in real PV power plants, MPPT algorithms are not performed continuously but with a certain frequency. The CMPP voltage has a clearly narrower range and much lower highest rates of change than the GMPP voltage. Thus, MPPT is expected to meet more difficulties when trying to follow the GMPP than the CMPP. Thus, in practice, the energy difference between the two MPPs would be somewhat smaller than the results of this study show. Considering nonidealities of practical MPPT was out of the scope of this study but taking them into account and studying how it affects the ESS sizing and differences between the GMPP and CMPP are other interesting topics for future studies increasing the practical value and importance of the results.

In real PV systems, DC-DC and DC-AC converters are used to connect the ESS to the DC or AC bus of the PV system and there are several connection configurations for both DC- and AC-connected ESSs.[27] The applied configuration affects overall system efficiency. In this study these converters and their efficiency were not taken into account. Moreover, the losses of the inverter were not taken into account. Considering these aspects is another topic for future research.

5. Conclusion

This article presented a study of sizing of DC- and AC-connected energy storage systems for power smoothing of PV strings. A scenario in which the MPP closest to the nominal MPP voltage was followed was compared to operation in the GMPP. The ESS was controlled to smooth the power fed to the grid to comply with certain RRL which was altered from 1 to 20% min^{-1} with respect to the nominal PV power. Moreover, the effects of inverter sizing were studied by altering DC/AC ratio from 0.8 to 2.0. The study was based on I–U curves of a 23 module PV string measured for 32 days.

The results demonstrate that it might be beneficial for PV systems to operate at the MPP closest to the nominal MPP voltage instead of the GMPP as the extremely wide operating voltage range when the GMPP is followed can be substantially reduced by that way at a cost of relatively small energy losses. It was found that following the CMPP instead of the GMPP increases the requirement for ESS discharging power capacity especially at low DC/AC ratios since the fastest rates of change in power are higher for the CMPP than for the GMPP. However, with typical DC/AC ratios of around 1.5, the practical meaning of the differences in power capacity requirements for a DC-connected ESS between the GMPP and CMPP is relatively small. Moreover, only minor differences were found in ESS energy capacity requirements between the GMPP and CMPP for both DC- and AC-connected ESSs. The results mean that, in practice, there are no major differences in sizing of DC-connected ESSs between the two MPPs.

Acknowledgements

The work was funded by the Research Council of Finland (funding decision 348701).

Conflict of Interest

The author declares no conflict of interest.

Author Contributions

Kari Lappalainen: Conceptualization (lead); Formal analysis (lead); Funding acquisition (lead); Investigation (lead); Methodology (lead); Writing—original draft (lead).

Data Availability Statement

The data that support the findings of this study are available from the corresponding author upon reasonable request.

Keywords

energy storage systems, inverter sizing, maximum power points, photovoltaics, power smoothing

Received: July 5, 2024
Revised: September 4, 2024
Published online:

[1] K. Lappalainen, S. Valkealahti, *Sol. Energy* **2015**, *112*, 55.
[2] K. Lappalainen, S. Valkealahti, *EPJ Photovoltaics* **2022**, *13*, 4.

[3] H. X. Wang, M. A. Munoz-García, G. P. Moreda, M. C. Alonso-García, *Renewable Energy* **2018**, *118*, 709.
[4] J. D. Mondol, Y. G. Yohanis, B. Norton, *Sol. Energy* **2006**, *80*, 1517.
[5] J. Zhu, R. Bründlinger, T. Mühlberger, T. R. Betts, R. Gottschalg, *IET Renewable Power Gener.* **2011**, *5*, 58.
[6] K. Lappalainen, J. Kleissl, *J. Renewable Sustainable Energy* **2020**, *12*, 043502.
[7] J. Luoma, J. Kleissl, K. Murray, *EPJ Photovoltaics* **2022**, *13*, 4.
[8] K. Lappalainen, S. Valkealahti, *Appl. Energy* **2021**, *301*, 117436.
[9] K. Lappalainen, J. Kleissl, in *Proc. of EU PVSEC 2023*, WIP Renewable Energies, Lisbon **2023**, https://doi.org/10.4229/EUPVSEC2023/5DV.2.6.
[10] W. C. S. Amorim, A. F. Cupertino, H. A. Pereira, V. F. Mendes, *Electr. Power Syst. Res.* **2024**, *229*, 110114.
[11] Y. Sun, Z. Zhao, M. Yang, D. Jia, W. Pei, B. Xu, *CSEE J. Power Energy Syst.* **2020**, *6*, 160.
[12] J. Martins, S. Spataru, D. Sera, D.-I. Stroe, A. Lashab, *Energies* **2019**, *12*, 1342.
[13] S. Sukumar, M. Marsadek, K. R. Agileswari, H. Mokhlis, *J. Energy Storage* **2018**, *20*, 218.
[14] M. Järvelä, S. Valkealahti, in *Proc. of IEEE 46th Photovoltaic Specialists Conf.*, IEEE, Chicago **2019**, https://doi.org/10.1109/PVSC40753.2019.8980909.
[15] K. Lappalainen, S. Valkealahti, *Renewable Energy* **2020**, *152*, 812.
[16] T. Esram, P. L. Chapman, *IEEE Trans. Energy Convers.* **2007**, *22*, 439.
[17] K. Lappalainen, S. Valkealahti, *IET Renewable Power Gener.* **2019**, *13*, 2864.
[18] H. Patel, V. Agarwal, *IEEE Trans. Energy Convers.* **2008**, *23*, 302.
[19] A. M. S. Furtado, F. Bradaschia, M. E. Cavalcanti, L. R. Limongi, *IEEE Trans. Ind. Electron.* **2018**, *65*, 3252.
[20] M. Boztepe, F. Guinjoan, G. Velasco-Quesada, S. Silvestre, A. Chouder, E. Karatepe, *IEEE Trans. Ind. Electron.* **2014**, *61*, 3302.
[21] K. Lappalainen, S. Valkealahti, in *Proc. of EU PVSEC 2021*, WIP Renewable Energies **2021**, p. 1264, https://doi.org/10.4229/EUPVSEC20212021-5CV.2.39.
[22] B. Yang, T. Zhu, J. Wang, H. Shu, T. Yu, X. Zhang, W. Yao, L. Sun, *J. Cleaner Prod.* **2020**, *268*, 121983.
[23] D. Mazumdar, C. Sain, P. Kumar Biswas, P. Sanjeevikumar, B. Khan, *Int. Trans. Electr. Energy Syst.* **2024**, *2024*, 8363342.
[24] A. Sangwongwanich, Y. Yang, F. Blaabjerg, in *Proc. of IEEE Energy Conversion Congress and Exposition*, IEEE, Milwaukee **2016**, https://doi.org/10.1109/ECCE.2016.7854671.
[25] D. Torres Lobera, A. Mäki, J. Huusari, K. Lappalainen, T. Suntio, S. Valkealahti, *Int. J. Photoenergy* **2013**, *2013*, 837310.
[26] K. Lappalainen, S. Valkealahti, *Renewable Energy* **2022**, *196*, 1366.
[27] J. Wang, K. Sun, C. Xue, T. Liu, Y. Li, *IEEE Trans. Ind. Electron.* **2022**, *69*, 4879.